Misfolded Opsin Mutants Display Elevated β -Sheet Structure

Lisa M. Miller, Megan Gragg, Tae Gyun Kim, Paul S.–H. Park

PII: S0014-5793(15)00812-1
DOI: http://dx.doi.org/10.1016/j.febslet.2015.08.042
Reference: FEBS 37352

To appear in: *FEBS Letters*

Received Date: 11 August 2015
Accepted Date: 31 August 2015

Please cite this article as: Miller, L.M., Gragg, M., Kim, T.G., Park, P.S., Misfolded Opsin Mutants Display Elevated β -Sheet Structure, *FEBS Letters* (2015), doi: http://dx.doi.org/10.1016/j.febslet.2015.08.042

Misfolded Opsin Mutants Display Elevated β-Sheet Structure

Lisa M. Miller[*,†], Megan Gragg[‡], Tae Gyun Kim[‡], and Paul S.–H. Park[*,‡]

[†] National Synchrotron Light Source-II, Brookhaven National Laboratory, Upton, NY 11973

[‡] Department of Ophthalmology and Visual Sciences, Case Western Reserve University, Cleveland, OH 44106

* To whom correspondence should be addressed:

Paul S.-H. Park, Department of Ophthalmology and Visual Sciences, Case Western Reserve University, Cleveland, OH 44106, USA, Ph: +1-216-368-2533; Fax: +1-216-368-3171; E-mail: paul.park@case.edu

Lisa M. Miller, National Synchrotron Light Source-II, Brookhaven National Laboratory, Upton, NY 11973. USA, Ph +1-631-344-2091; Fax: +1-631-344-7039; E-mail: lmiller@bnl.gov

Abstract

Mutations in rhodopsin can cause misfolding and aggregation of the receptor, which leads to retinitis pigmentosa, a progressive retinal degenerative disease. The structure adopted by misfolded opsin mutants and the associated cell toxicity is poorly understood. Förster resonance energy transfer (FRET) and Fourier transform infrared (FTIR) microspectroscopy were utilized to probe within cells the structures formed by G188R and P23H opsins, which are misfolding mutants that cause autosomal dominant retinitis pigmentosa. Both mutants formed aggregates in the endoplasmic reticulum and exhibited altered secondary structure with elevated β-sheet and reduced α-helical content. The newly formed β-sheet structure may facilitate the aggregation of misfolded opsin mutants. The effects observed for the mutants were unrelated to retention of opsin molecules in the endoplasmic reticulum itself.

Keywords:

G protein-coupled receptor, membrane protein, protein aggregation, protein misfolding, secondary structure, retinal degeneration

Abbreviations:

CD, circular dichroism; CFP, cyan fluorescent protein; DM, *n*-Dodecyl-β-D-maltoside; ER, endoplasmic reticulum; FRET, Förster resonance energy transfer; FTIR, Fourier transform infrared (FTIR); GPCR, G protein-coupled receptor; MII, metarhodopsin II; mRho, murine rhodopsin; mTq, mTurquoise; PCR, polymerase chain reaction; RP, retinitis pigmentosa; WGA, wheat germ agglutinin; WT, wild-type; WT-KKYL, wild-type with an ER retention sequence; YFP, yellow fluorescent protein

1. Introduction

Retinitis pigmentosa (RP) is a hereditary and progressive retinal degenerative disease that can be caused by defects in different genes [1, 2]. Mutations in the gene for rhodopsin, the light receptor in rod photoreceptor cells that initiates vision via phototransduction, are the largest genetic cause of autosomal dominant RP [1]. Over 100 mutations in rhodopsin have been detected in patients with RP [2, 3]. A majority of these mutations cause misfolding of the apoprotein opsin, a membrane protein with 7 α-helical transmembrane domains, and an inability to bind the chromophore 11-*cis* retinal [4, 5]. Misfolded opsin mutants are improperly targeted in the cell and retained in the endoplasmic reticulum (ER) forming aggregates [6, 7]. Thus, RP can be classified as a protein conformational or protein misfolding disease.

Misfolded opsin mutants that cause RP are often presumed to form amorphous aggregates [8], which can cause ER stress leading to cell death. A large number of conformational diseases are caused by toxic amyloid-type aggregates [9, 10]. Thus far, only amyloid-type aggregates formed by peptides or globular proteins have been detected and studied. It is unclear whether or not membrane proteins like opsin can also form aggregates that share features displayed by amyloids. While aggregation underlies the toxicity of misfolded opsin mutants [6, 11], the structures adopted by misfolded opsins and the resulting aggregates are unknown. The limited structural information about misfolded opsin mutants have been inferred from receptors extracted from the cell using detergent [12]. Structural insights on misfolded opsin mutants within the context of the cell are absent.

The structural characterization of membrane proteins presents a challenge since they require a lipid bilayer for stabilization and function. Conventional approaches are often not amenable for examining the structure of membrane proteins under physiologically relevant conditions. In

contrast, Förster resonance energy transfer (FRET) and Fourier transform infrared (FTIR) microspectroscopy can provide structural information about membranes proteins within the native context of the cell [13, 14]. Thus, FRET and FTIR microspectroscopy were utilized in the current study to investigate the structural changes accompanying misfolded mutants of opsin within the cell.

2. Materials and Methods

2.1 DNA Constructs

SCFP3A and mTurquoise (mTq) are variants of cyan fluorescent protein (CFP) and SYFP2 is a variant of yellow fluorescent protein (YFP). The vectors pSCFP3A-N1, pSYFP2-N1, and pmTq-C1 were generated as described previously [14, 15]. The sequence 5'-ACGGAGACCAGCCAGGTGGCTCCAGCCTAA-3', which corresponds to a 1D4 epitope (TETSQVAPA) [16], was added to the end of the sequences for SCFP3A or SYFP2 by PCR amplification using pSCFP3A-N1 and pSYFP2-N1 as templates, generating the products SCFP3A-1D4 and SYFP2-1D4, respectively. The sequences for the fluorescent proteins in pSCFP3A-N1 and pSYFP2-N1 were replaced with the PCR amplified SCFP3A-1D4 and SYFP2-1D4 to generate the vectors pSCPF3A-1D4-N1 and pSYFP2-1D4-N1, respectively. The cDNA for murine rhodopsin (mRho) was amplified by PCR to include an EcoRI restriction endonuclease site and Kozak sequence at the 5' end and a BamHI restriction endonuclease site at the 3' end of the sequence with the stop codon removed. This amplified mRho sequence was inserted into pSCPF3A-1D4-N1 and pSYFP2-1D4-N1 at the EcoRI and BamHI restriction endonuclease sites to generate the vectors pmRho-SCFP3A-1D4 and pmRho-SYFP2-1D4. To generate vectors for tagged rhodopsin containing an ER retention sequence, the sequence 5'-

ACTTTAGCTTCTTCTTTAACTTTCAAGAAGTATCTTTAA-3', which contains a KKYL ER retention sequence [17], was added to the end of the sequences for mTq or SYFP2 by PCR using vectors containing sequences for these fluorescent proteins as the template. SYFP2-1D4 in pmRho-SYFP-1D4 was replaced by either the PCR products mTq-KKYL or SYFP2-KKYL to generate the vectors pmRho-mTq-KKYL and pmRho-SYFP2-KKYL. To generate a vector for the expression of untagged rhodopsin, the cDNA for mRho was amplified by PCR to include an EcoRI restriction endonuclease site and Kozak sequence at the 5' end and a NotI restriction endonuclease site at the 3' end. This amplified PCR product was inserted into pSCFP3A-N1 at the EcoRI and NotI restriction endonuclease sites, which replaced the sequence for the fluorescence protein with the mRho sequence to generate the vector pmRho. The P23H and G188R mutations were introduced adapting procedures in the QuickChange II Site-Directed Mutagenesis Kit (Agilent Technologies, Santa Clara, CA). The following primers were used: P23H-forward, 5'-GTGCGGAGCCACTTCGAGCAG-3'; P23H-reverse, 5'-CTGCTCGAAGTGGCTCCGCCAC-3'; G188R-forward, 5'-TGTTCATGCAGGATTGACTAC-3'; G188R-reverse, 5'-GTAGTCAATCCTGCATGAACA-3'. The vectors generated were used for transient transfection of HEK293 cells.

2.2 Transient Transfection of HEK293 Cells

HEK293T/17 cells (American Type Culture Collection, Manassas, VA) were grown in Dulbecco's Modified Eagle's Medium (DMEM)-high glucose (Thermo Fisher Scientific, Waltham, MA), supplemented with 10% fetal bovine serum (Thermo Fisher Scientific, Waltham, MA). Prior to transfection, HEK 293T/17 cells were seeded in a 12 well plate at a density of 1.5 x 10^5 cells per well. Cells used for confocal imaging were seeded on poly-L-lysine treated #1.5

coverslip glass (Thermo Fisher Scientific, Waltham, MA). Cells used for FTIR were seeded on 13 x 1 mm CaF_2 discs (Crystran Limited, Poole, United Kingdom). Cells were incubated in a 5% CO_2 incubator for 24 h, after which cells reached 60% confluency. Transfection of cells with DNA vectors described earlier was performed using Lipofectamine 2000 (Invitrogen, Carlsbad, CA). 200 ng of a single DNA vector or 200 ng each of two DNA vectors were used in transfections and cotransfections, respectively. For studies requiring visualization of the ER, cells were cotransfected with 1000 ng of the vector pDsRed2-ER (Clontech, Mountain Valley, CA), which codes for an ER marker. 24 h post-transfection, the media was removed and each well was washed once with 1 mL PBS (4.3 mM $Na_2HPO_4 \cdot 7H_2O$, 1.4 mM KH_2PO_4, 137 mM NaCl, 2.7 mM KCl, pH 7.3). For FRET assays, cells were resuspended in 3 mL of PBS.

2.3 Confocal Microscopy

Cells on coverslips were fixed in 4% paraformaldehyde for 10 min at room temperature. Cells were washed with PBS three times. The plasma membrane was stained by wheat germ agglutinin (WGA)-Alexa Fluor 647 conjugate (Invitrogen, Carlsbad, CA) at a 1:200 dilution for 10 min at room temperature. Cells were washed three times with PBS. Cell nuclei were stained with 0.5 μg/mL of DAPI for 10 min at room temperature. Cells were washed twice with PBS and once with water. Coverslips were mounted on a glass slide using ProLong Gold Antifade Mountant (Life Technologies, Eugene, OR). Confocal microscopy was performed on a SP8 confocal microscope (Leica, Buffalo Grove, IL) equipped with a 100x/1.4-NA oil objective. DAPI was detected by exciting samples with a 405 nm diode laser and collecting the emission signal at 415 – 430 nm. YFP was detected by exciting samples at 514 nm using a tunable white light laser and collecting the emission signal at 520 – 560 nm. WGA-Alexa Fluor 647 was

detected by exciting samples at 650 nm using a tunable white light laser and collecting the emission signal at 660 – 680 nm. DsRed2-ER was detected by exciting samples at 558 nm using a tunable white laser and collecting the emission signal at 570-600 nm.

2.4 FRET Assay

FRET assays on cell suspensions were conducted on a FluoroMax-4 spectrofluorometer (Horiba Jobin Yvon, Edison, NJ). Samples were excited at 425 nm with a 5 nm excitation slit width to excite CFP. The emission spectra were obtained with a 10 nm emission slit width. All samples were maintained at 25 °C with a circulating water bath. The samples were then treated 5 min with 1.3 mM *n*-dodecyl-β-D-maltoside (DM, Anatrace, Maumee, OH) and 5 min with 3.3 mM SDS (Invitrogen, Carlsbad, CA). After each detergent treatment step, the fluorescence spectra were obtained again. Background was computed using negative control cells coexpressing untagged opsin and YFP-tagged opsin.

2.5 FTIR Microspectroscopy

FTIR microspectroscopy was performed using a Thermo Nicolet Continuum IR microscope coupled to beamline U2B at the National Synchrotron Light Source (NSLS) at Brookhaven National Laboratory (Upton, NY). Additional spectra were collected at beamline 1.4.4 at the Advanced Light Source (ALS) at Lawrence Berkeley National Laboratory (Berkeley, CA). In both cases, a 32x IR Schwarzchild objective produced a 10 x 10 μm beam. A 4 cm^{-1} spectral resolution and 128 scans per spectrum were used over the mid-infrared region (4000 – 800 cm^{-1}). For each transfected cell type, spectra were collected from regions of 40-50 cells that exhibited bright fluorescence from YFP. For transfected cells using constructs without YFP, spectra were

collected from all areas of the cell and were manually sorted. Thus, spectra of untagged opsins are not as reliable as those from tagged opsins since the absence of fluorescence from YFP prevented an accurate localization of the opsins in the cell. Spectra were also collected from untransfected cells. Spectra shown in the figures represent the averages of the 40-50 spectra. For each average spectrum, the β-sheet/amide I ratio and the α-helix/amide I ratio were calculated by integrating the β-sheet component (1625 – 1630 cm^{-1}) or α-helix component (1650 – 1655 cm^{-1}) and ratioing to the amide I band area (1600 – 1700 cm^{-1}) using a linear baseline from 1480 to 1800 cm^{-1}. The integrated values for the β-sheet component and α-helix component were also used to compute the β-sheet/α-helix ratio.

2.6 Generation of Stable HEK293 Cell Lines

Stable HEK293 cell lines expressing mRho, mRho-SCFP3A-1D4, or mRho-SYFP2-1D4 were generated using the Flp-In System (Invitrogen, Carlsbad, CA). The cDNA for mRho, mRho-SCFP3A-1D4, and mRho-SYFP2-1D4 were subcloned from the vectors pmRho, pmRho-SCFP3A-1D4, and pmRho-SCFP3A-1D4 into the vector pcDNA5/FRT at the NheI and NotI restriction endonuclease sites.

2.7 Reconstitution and Purification of Isorhodopsin

Stable HEK293 cell lines expressing mRho, mRho-SCFP3A-1D4, or mRho-SYFP2-1D4 were grown in DMEM-high glucose supplemented with 10% fetal bovine serum on 100 x 20 mm tissue culture plates. For each purified preparation, cells were grown to confluency, harvested from 10 to 30 plates, and resuspended in 4 mL of PBS supplemented with a protease inhibitor cocktail tablet (Roche Diagnostics, Indianapolis, IN). All reconstitution and purification

procedures were performed in the dark or under dim red light conditions. Opsin expressed in the stable HEK293 cells was reconstituted with 9-*cis* retinal (Sigma-Aldrich, St. Louis, MO). A stock solution of 9-*cis* retinal in DMSO (100 mM) was added to the cell suspension to achieve a final concentration of 100 μM. The cell suspension with chromophore was shaken at room temperature for 2 h. Reconstituted cells were pelleted by centrifugation at 90,000 x g for 10 min at 4 °C. The cell pellet was resuspended and homogenized in 10 mM Bis-Tris propane, 500 mM NaCl, 20 mM DM, pH 7.5 supplemented with a protease inhibitor cocktail tablet. The cell suspension was shaken at room temperature for 15 min and then centrifuged at 90,000 x g for 20 min at 4 °C. The supernatant was loaded on a 6 × 30 mm column packed with Sepharose 4B (Santa Cruz Biotechnology, Santa Cruz, CA) coupled to anti-1D4 antibody [16]. Isorhodopsin was purified as described previously [18].

2.8 UV-Visible Absorbance Spectroscopy

Absorbance spectra of purified isorhodopsin were obtained using a Lambda 35 UV-visible spectrophotometer (PerkinElmer, Waltham, MA). Hydroxylamine hydrochloride was added from a 1 M (pH 7.0) stock solution to purified samples to achieve a final concentration of 20 mM. A first absorbance spectrum was obtained using buffer as a blank. A difference spectrum was then obtained by using the unbleached sample as the blank, bleaching the sample for 5 min using a MI-150 Fiber-Lite illuminator (Dolan-Jenner Industries, Boxborough, MA) equipped with a 480-520 nm band-pass filter, and then reading the bleached sample.

2.9 MII Decay Assay

Purified isorhodopsin was investigated in 20 mM Bis-Tris propane, 120 mM NaCl, 2 mM DM, pH 6.0. Samples were bleached for 15 s using a MI-150 Fiber-Lite illuminator equipped with a 480-520 nm band-pass filter. Intrinsic tryptophan fluorescence was then measured over time on a FluroMax-4 spectrofluorometer by using an excitation wavelength of 295nm (1 nm slit width) and emission wavelength of 330 nm (10 nm slit width). A circulating water bath was used to maintain a constant sample temperature of 20 °C. The increase in tryptophan fluorescence correlates with the release of *all*-trans-retinal from the binding pocket of rhodopsin occurring upon the decay of the active MII state [19]. Fluorescence data were analyzed by nonlinear regression fitting to an exponential one-phase decay equation in Prism 6 (GraphPad Software, La Jolla, CA). Two different preparations were tested for purified untagged, CFP-tagged, and YFP-tagged isorhodoopsin.

3. Results and Discussion

3.1 Characterization of tagged opsins expressed in HEK293 cells

The opsin mutants investigated in the current study contain the G188R and P23H mutations. The P23H mutation in opsin was the first one discovered to cause autosomal dominant RP in patients and is the most common RP-causing mutation in opsin in the United States [20]. The G188R mutation in opsin also causes autosomal dominant RP [21]. Both point mutations cause misfolding of opsin [12, 22]. Wild-type (WT), G188R, and P23H opsins were expressed in HEK293 cells. Expression of mutant opsins in cultured cells such as HEK293 or COS-1 cells has served as a good model system to examine protein misfolding and preciliary targeting events [23]. Opsins were tagged at the C-terminus with variants of the fluorescent proteins cyan

fluorescent protein (CFP) or yellow fluorescent protein (YFP) for visualization of the receptors in the cell and for FRET studies [24].

To test whether or not tagging opsin with fluorescent proteins impacts protein folding or function, the ability to bind chromophore and receptor activation were investigated. Only properly folded opsin can covalently bind the chromophore 11-*cis* retinal to form rhodopsin. To determine the ability of tagged WT opsin to bind chromophore, the apoprotein was reconstituted with a more stable isomer of 11-*cis* retinal, 9 *cis*-retinal. The binding of 9 *cis*-retinal to opsin forms isorhodopsin, which is functionally similar to rhodopsin except for a blue-shifted absorbance maximum of 487 nm [25]. Purified untagged opsin expressed in HEK293 cells and reconstituted with 9-*cis* retinal exhibited the characteristic absorbance maximum for isorhodopsin at 487 nm (Fig. 1A). Purified opsins tagged with either CFP or YFP displayed complex absorbance spectra due to contributions from both isorhodopsin and the fluorescent proteins (Figs. 1B and 1C). To separate out the component corresponding to isorhodopsin, difference spectra were recorded after bleaching samples. The difference spectra displayed minima at 487 nm, thereby indicating that both CFP- and YFP- tagged opsins bind 9-*cis* retinal.

Activation of rhodopsin or isorhodopsin occurs after the light-induced isomerization of 11-*cis* retinal or 9-*cis* retinal to all-*trans* retinal [26]. This isomerization of bound chromophore is evident in the difference absorbance spectra collected after bleaching samples. The disappearance of absorbance derived from 9-*cis* retinal at 487 nm is accompanied by the appearance of absorbance derived from all-*trans* retinal at 368 nm (Figs. 1A-1C). The active state of rhodopsin or isorhodopsin, referred to as metarhodopsin II (MII), decays by releasing all-*trans* retinal from the binding pocket in opsin. The MII decay rate was determined for untagged and tagged isorhodopsin by monitoring the dequenching of a tryptophan residue that correlates

with the release of all-*trans* retinal from the binding pocket in opsin of the MII state [19]. The MII state of untagged isorhodopsin decayed with a time constant of 22 min (Fig. 1D). The MII states of CFP- and YFP-tagged isorhodopsin displayed similar decay rates that were about 1.3-fold slower than that observed for untagged isorhodopsin (Figs. 1E and 1F). In previous studies, fluorescent proteins were shown not to impact the ability of the receptor to activate transducin or become phosphorylated by rhodopsin kinase [27]. Taken together, receptor tagged with either CFP or YFP are functional, although the additional mass of the attached fluorescent protein slows down the rate of MII decay somewhat.

The localization of tagged WT, G188R, and P23H opsins in transfected HEK293 cells was investigated by confocal microscopy. Wheat germ agglutinin (WGA) was used to stain the plasma membrane (Figs. 2A-2C) and an ER marker was coexpressed to determine ER localization (Figs. 2E-2G). As shown previously [4, 6, 7], WT opsin was properly targeted to the plasma membrane and largely excluded from the ER whereas the G188R and P23H mutants were mislocalized and retained in the ER (Fig. 2). The retention of mutant receptors in the ER of HEK293 cells recapitulates the effects observed in photoreceptor cells of the retina [28-30], although a larger fraction of the misfolded receptor is rapidly degraded in photoreceptor cells compared to that in cultured cells [31].

3.2 Differentiating between oligomers and aggregates of opsin in HEK293 cells

Natively, rhodopsin and opsin in photoreceptor cells form oligomers organized into nanodomains that can be disrupted by the mild detergent *n*-Dodecyl-*β*-D-maltoside (DM) [32-35]. Oligomers of tagged rhodopsin and opsin have also been detected in COS-1 and HEK293 cells and liposomes by FRET approaches [6, 36-38]. Similar to native conditions, oligomers of

rhodopsin in heterologous expression systems are disrupted by DM [38]. Consistent with these previous studies, CFP- and YFP-tagged WT opsin co-expressed in HEK293 cells exhibited FRET that could be disrupted by treatment with DM (Fig. 2I). FRET has also been used previously to investigate the interactions between P23H opsins in HEK293 cells [6]; however, monitoring the FRET signal alone cannot differentiate between oligomers normally formed by WT opsin versus non-native oligomers (i.e., aggregates) formed by misfolded opsins. Coexpression of CFP- and YFP-tagged misfolded opsin mutants in HEK293 cells exhibited FRET; however, the FRET signal could not be completely eliminated by treatment with DM (Figs. 2J and 2K). The stronger detergent SDS was required to fully disrupt the FRET signal. Thus, the sensitivity of the FRET signal to DM treatment allows for the differentiation between misfolded mutant aggregates and normal opsin oligomers.

To determine whether or not retention in the ER itself promotes aggregation of opsin, YFP-tagged WT opsin with an ER retention sequence (WT-KKYL) was expressed in HEK293 cells and investigated [17]. Similar to the mutant opsins, tagged WT-KKYL opsin was localized in the ER and excluded from the plasma membrane (Figs. 2D and 2H). FRET studies were conducted to determine if WT-KKYL opsin forms oligomers or aggregates. FRET was observed in cells coexpressing CFP- and YFP-tagged WT-KKYL opsin, which was disrupted by treatment with DM (Fig. 2L). FRET results of WT-KKYL opsin are more similar to those of WT opsin than to those of the mutant opsins. Thus, the retention of WT opsin in the ER does not promote aggregation.

3.3 Secondary structure changes in misfolded opsin mutants

The nature of the structure adopted by misfolded opsin mutants in HEK293 cells was investigated by synchrotron FTIR microspectroscopy. FTIR spectroscopy is a widely used technique for determining the secondary structure of proteins and synchrotron-based FTIR microspectroscopy enables the localization of these structures within a cell at subcellular resolution and with a high signal-to-noise ratio [13, 39]. In this study, FTIR spectra were obtained from cells grown on CaF_2 discs. Spectra were collected from regions in the cell exhibiting bright fluorescence from YFP (e.g., Fig. 3A).

In all cells, the two most prominent peaks in the FTIR spectra were the amide I (1650 cm^{-1}) and amide II (1550 cm^{-1}) protein bands (Figs. S1-S3). The amide I band contains much of the secondary structure information about proteins [39]. α-helices and β-sheets exhibit absorbance in the spectra at 1655 cm^{-1} and 1630 cm^{-1}, respectively. Transforming the absorbance spectra into second derivative spectra provides more detailed and resolved spectra [39]. Results showed a difference in the amide I band of FTIR spectra collected from untransfected cells and cells expressing YFP-tagged WT opsin, which included an increase in absorbance at 1630 cm^{-1} for cells expressing tagged WT opsin (Fig. 3D). The second derivative spectrum displayed a clear change in absorbance at 1630 cm^{-1} for cells expressing tagged WT opsin (Fig. 3C), which was indicative of an increase in β-sheet structure. A similar change was also observed in this region of the spectrum in cells expressing YFP alone. Since YFP has a β-barrel structure, the increase in absorbance at 1630 cm^{-1} observed in cells expressing tagged WT opsin likely derives from the β-sheet structure of the attached YFP rather than the structure of opsin. Consistent with this prediction, the FTIR spectrum for untagged WT opsin was similar to that of untransfected HEK293 cells at 1630 cm^{-1}.

Cells expressing YFP-tagged forms of either the G188R or P23H mutants displayed an even greater increase in absorbance at 1630 cm^{-1} compared to cells expressing YFP-tagged WT opsin (Fig. 3E and 3F). This increased absorbance for the mutants points to changes in the secondary structure of the opsin molecule itself. This was confirmed by examining cells expressing untagged opsin mutants, which also displayed an increase in absorbance at 1630 cm^{-1} (Figs. 3G and 3H). Furthermore, when mapping the β-sheet content in the HEK293 cells, regions with elevated β-sheet content were clearly co-localized with the bright YFP fluorescence signal from tagged misfolded opsins (Figs. 3A and 3B). Elevated β-sheet content was not observed in maps of HEK293 cells expressing tagged WT opsin. Retention of opsin in the ER itself did not result in elevated β-sheet content as the FTIR spectrum for YFP-tagged WT-KKYL opsin was similar as that for tagged WT opsin at 1630 cm^{-1} (Figs. 3E and 3F).

The change in secondary structure of the misfolded mutants was quantified by calculating the β-sheet/α-helix ratio from FTIR spectra and comparing this value with that computed from the WT opsin spectrum. A 14% and 24 % increase in β-sheet content relative to α-helical content was observed in spectra for the G188R and P23H mutants, respectively. This increase resulted from both an increase in β-sheet structure and decrease in α-helical structure in cells expressing the mutants compared to those expressing WT opsin. A 7% increase in β-sheet structure and 6% decrease in α-helical structure were observed for G188R opsin and a 14% increase in β-sheet structure and 8% decrease in α-helical structure were observed for P23H opsin. In contrast, no change in α-helical and β-sheet structure was detected for tagged WT-KKYL. Thus, a conversion of α-helical structure to β-sheet structure appears to occur in the mutant opsins that is unrelated to the retention of opsin molecules in the ER.

The changes in secondary structure of misfolded opsins detected in transfected HEK293 cells are consistent with previous in vitro studies on purified receptors. A decrease in α-helical structure and increase in β-sheet structure has been observed previously by infrared reflection absorption spectroscopy in purified rhodopsin induced to unfold by environmental perturbation [40]. Thus, misfolding of opsin promoted by mutation or environmental perturbations may result in similar secondary structure changes. A change in secondary structure has also been observed previously by circular dichroism (CD) spectroscopy on detergent-solubilized and purified G188R and P23H opsins [12]. CD spectroscopy revealed that the purified mutant opsins had a 25% reduction in α-helical content compared to properly folded purified opsin [12]. The partial reduction in α-helical content indicates that the misfolded mutants only partially misfold and retain the majority of native secondary structure. Since FTIR spectroscopy is better suited at detecting β-sheet structure compared to CD spectroscopy and can also be used to determine α-helical content [39], changes in both α-helical and β-sheet structure were observed in the current study whereas only changes in α-helical structure were detectable by CD spectroscopy. The G188R and P23H mutations appear to cause localized perturbations where β-sheet structure is formed at least in part by conversion from native α-helical structure. Future FTIR studies on purified receptors will be required to quantitatively assess changes in misfolded mutant opsin secondary structure and to exclude secondary effects occurring in the ER that may contribute to the FTIR spectrum obtained from a cell.

3.4 Implications of elevated β-sheet structure in opsin mutants

Aggregation of misfolded opsin mutants is not a result of non-specific interactions of hydrophobic proteins, but rather, mediated by specific interactions [41]. The detection of

elevated β-sheet structure in opsin mutants may provide a clue to how this specificity is achieved. Increased β-sheet structure is characteristic of a wide range of peptides and globular proteins that form amyloids, which are toxic to cells and cause a variety of diseases including progressive neurodegenerative conditions such as Alzheimer's disease, Huntington's disease, Parkinson's disease, and amyotrophic lateral sclerosis [9, 10]. β-sheets mediate the interactions between monomeric peptides or misfolded globular proteins to form amyloid oligomers or fibrils. Similar to amyloid-forming proteins, opsin mutants display increased β-sheet structure and aggregation. Thus, the specificity of misfolded mutant opsin aggregates may be achieved by defined binding interfaces involving β-sheets. The structures of misfolded opsin mutant aggregates are likely distinct from those of amyloids, however, since staining is not observed by thioflavin T or the anti-oligomer antibody A11 (data not shown), which bind generic structures present in amyloid fibrils and oligomers [42-44].

The similarities in effects observed for G188R and P23H opsins suggest that all misfolded opsin mutants that cause RP may undergo similar types of structural changes and aggregation. Moreover, misfolding of opsin promoted by environmental factors may also cause similar structural transitions in the receptor as that caused by mutation [40]. Findings from the current study may have even broader implications. Rhodopsin is a prototypical member of the G protein-coupled receptor (GPCR) family of cell surface receptors, one of the largest classes of proteins and therapeutic targets. Heritable mutations are also found in other GPCRs that cause receptor misfolding, which results in disorders such as hypogonadism, diabetes, and obesity [45]. The structure of these misfolded mutant GPCRs and their propensity to form aggregates is unknown. Commonalities in the structure of GPCRs raise the possibility that increased β-sheet structure

and specific aggregation may be a common feature for all members of this family of proteins that are prone to misfold when destabilizing mutations are introduced.

Acknowledgements

We would like to thank Dawn Smith for culturing HEK293 cells, Patricia Conrad for training on the confocal microscope, and Theodorus W. J. Gadella (University of Amsterdam, Amsterdam, Netherlands) for providing the vector containing the cDNA for mTurquoise. This work was funded by grants from the National Institutes of Health (R01EY021731, P30EY011373, and T32EY024236) and Research to Prevent Blindness (Unrestricted Grant and Career Development Award). The National Synchrotron Light Source and the Advanced Light Source are supported by the US Department of Energy contract Nos. DE-AC02-98CH10886 and DE-AC02-05CH11231, respectively. We would like to acknowledge use of the Leica SP8 confocal microscope in the Genetics Department Imaging Facility at Case Western Reserve University made available through the Office of Research Infrastructure Programs (NIH-ORIP) Shared Instrumentation Grant S10 OD016164.

References

1. Hartong, D. T., Berson, E. L. & Dryja, T. P. (2006) Retinitis pigmentosa, *Lancet.* **368**, 1795-809.

2. Daiger, S. P., Sullivan, L. S. & Bowne, S. J. (2013) Genes and mutations causing retinitis pigmentosa, *Clin Genet.* **84**, 132-41.

3. Mendes, H. F., van der Spuy, J., Chapple, J. P. & Cheetham, M. E. (2005) Mechanisms of cell death in rhodopsin retinitis pigmentosa: implications for therapy, *Trends Mol Med.* **11**, 177-85.

4. Sung, C. H., Davenport, C. M. & Nathans, J. (1993) Rhodopsin mutations responsible for autosomal dominant retinitis pigmentosa. Clustering of functional classes along the polypeptide chain, *J Biol Chem.* **268**, 26645-9.

5. Krebs, M. P., Holden, D. C., Joshi, P., Clark, C. L., 3rd, Lee, A. H. & Kaushal, S. (2010) Molecular mechanisms of rhodopsin retinitis pigmentosa and the efficacy of pharmacological rescue, *J Mol Biol.* **395**, 1063-78.

6. Illing, M. E., Rajan, R. S., Bence, N. F. & Kopito, R. R. (2002) A rhodopsin mutant linked to autosomal dominant retinitis pigmentosa is prone to aggregate and interacts with the ubiquitin proteasome system, *J Biol Chem.* **277**, 34150-60.

7. Saliba, R. S., Munro, P. M., Luthert, P. J. & Cheetham, M. E. (2002) The cellular fate of mutant rhodopsin: quality control, degradation and aggresome formation, *J Cell Sci.* **115**, 2907-18.

8. Surguchev, A. & Surguchov, A. (2010) Conformational diseases: looking into the eyes, *Brain Res Bull.* **81**, 12-24.

9. Chiti, F. & Dobson, C. M. (2006) Protein misfolding, functional amyloid, and human disease, *Annu Rev Biochem.* **75**, 333-66.

10. Knowles, T. P., Vendruscolo, M. & Dobson, C. M. (2014) The amyloid state and its association with protein misfolding diseases, *Nat Rev Mol Cell Biol.* **15**, 384-96.

11. Bence, N. F., Sampat, R. M. & Kopito, R. R. (2001) Impairment of the ubiquitin-proteasome system by protein aggregation, *Science.* **292**, 1552-5.

12. Liu, X., Garriga, P. & Khorana, H. G. (1996) Structure and function in rhodopsin: correct folding and misfolding in two point mutants in the intradiscal domain of rhodopsin identified in retinitis pigmentosa, *Proc Natl Acad Sci U S A.* **93**, 4554-9.

13. Miller, L. M., Bourassa, M. W. & Smith, R. J. (2013) FTIR spectroscopic imaging of protein aggregation in living cells, *Biochim Biophys Acta.* **1828**, 2339-46.

14. Hovan, S. C., Howell, S. & Park, P. S. (2010) Forster resonance energy transfer as a tool to study photoreceptor biology, *J Biomed Opt.* **15**, 067001.

15. Goedhart, J., van Weeren, L., Hink, M. A., Vischer, N. O., Jalink, K. & Gadella, T. W., Jr. (2010) Bright cyan fluorescent protein variants identified by fluorescence lifetime screening, *Nat Methods.* **7**, 137-9.

16. Molday, R. S. & MacKenzie, D. (1983) Monoclonal antibodies to rhodopsin: characterization, cross-reactivity, and application as structural probes, *Biochemistry.* **22**, 653-60.

17. Zerangue, N., Malan, M. J., Fried, S. R., Dazin, P. F., Jan, Y. N., Jan, L. Y. & Schwappach, B. (2001) Analysis of endoplasmic reticulum trafficking signals by combinatorial screening in mammalian cells, *Proc Natl Acad Sci U S A.* **98**, 2431-6.

18. Kawamura, S., Colozo, A. T., Muller, D. J. & Park, P. S. (2010) Conservation of molecular interactions stabilizing bovine and mouse rhodopsin, *Biochemistry.* **49**, 10412-20.

19. Farrens, D. L. & Khorana, H. G. (1995) Structure and function in rhodopsin. Measurement of the rate of metarhodopsin II decay by fluorescence spectroscopy, *J Biol Chem.* **270**, 5073-6.

20. Dryja, T. P., McGee, T. L., Reichel, E., Hahn, L. B., Cowley, G. S., Yandell, D. W., Sandberg, M. A. & Berson, E. L. (1990) A point mutation of the rhodopsin gene in one form of retinitis pigmentosa, *Nature.* **343**, 364-6.

21. Dryja, T. P., Hahn, L. B., Cowley, G. S., McGee, T. L. & Berson, E. L. (1991) Mutation spectrum of the rhodopsin gene among patients with autosomal dominant retinitis pigmentosa, *Proc Natl Acad Sci U S A.* **88**, 9370-4.

22. Iannaccone, A., Man, D., Waseem, N., Jennings, B. J., Ganapathiraju, M., Gallaher, K., Reese, E., Bhattacharya, S. S. & Klein-Seetharaman, J. (2006) Retinitis pigmentosa associated with rhodopsin mutations: Correlation between phenotypic variability and molecular effects, *Vision Res.* **46**, 4556-67.

23. McKeone, R., Wikstrom, M., Kiel, C. & Rakoczy, P. E. (2014) Assessing the correlation between mutant rhodopsin stability and the severity of retinitis pigmentosa, *Mol Vis.* **20**, 183-99.

24. Kremers, G. J., Goedhart, J., van Munster, E. B. & Gadella, T. W., Jr. (2006) Cyan and yellow super fluorescent proteins with improved brightness, protein folding, and FRET Forster radius, *Biochemistry.* **45**, 6570-80.

25. Hubbard, R. & Wald, G. (1952) Cis-trans isomers of vitamin A and retinene in the rhodopsin system, *J Gen Physiol.* **36**, 269-315.

26. Park, P. S. (2014) Constitutively active rhodopsin and retinal disease, *Advances in pharmacology.* **70**, 1-36.

27. Jin, S., McKee, T. D. & Oprian, D. D. (2003) An improved rhodopsin/EGFP fusion protein for use in the generation of transgenic Xenopus laevis, *FEBS Lett.* **542**, 142-6.

28. Price, B. A., Sandoval, I. M., Chan, F., Simons, D. L., Wu, S. M., Wensel, T. G. & Wilson, J. H. (2011) Mislocalization and degradation of human P23H-rhodopsin-GFP in a knockin mouse model of retinitis pigmentosa, *Invest Ophthalmol Vis Sci.* **52**, 9728-36.

29. Tam, B. M. & Moritz, O. L. (2006) Characterization of rhodopsin P23H-induced retinal degeneration in a Xenopus laevis model of retinitis pigmentosa, *Invest Ophthalmol Vis Sci.* **47**, 3234-41.

30. Frederick, J. M., Krasnoperova, N. V., Hoffmann, K., Church-Kopish, J., Ruther, K., Howes, K., Lem, J. & Baehr, W. (2001) Mutant rhodopsin transgene expression on a null background, *Invest Ophthalmol Vis Sci.* **42**, 826-33.

31. Sakami, S., Maeda, T., Bereta, G., Okano, K., Golczak, M., Sumaroka, A., Roman, A. J., Cideciyan, A. V., Jacobson, S. G. & Palczewski, K. (2011) Probing mechanisms of photoreceptor degeneration in a new mouse model of the common form of autosomal dominant retinitis pigmentosa due to P23H opsin mutations, *J Biol Chem.* **286**, 10551-67.

32. Liang, Y., Fotiadis, D., Filipek, S., Saperstein, D. A., Palczewski, K. & Engel, A. (2003) Organization of the G protein-coupled receptors rhodopsin and opsin in native membranes, *J Biol Chem.* **278**, 21655-21662.

33. Jastrzebska, B., Maeda, T., Zhu, L., Fotiadis, D., Filipek, S., Engel, A., Stenkamp, R. E. & Palczewski, K. (2004) Functional characterization of rhodopsin monomers and dimers in detergents, *J Biol Chem.* **279**, 54663-75.

34. Whited, A. M. & Park, P. S. (2015) Nanodomain organization of rhodopsin in native human and murine rod outer segment disc membranes, *Biochim Biophys Acta.* **1848**, 26-34.

35. Rakshit, T. & Park, P. S. (2015) Impact of reduced rhodopsin expression on the structure of rod outer segment disc membranes, *Biochemistry.* **54**, 2885-94.

36. Mansoor, S. E., Palczewski, K. & Farrens, D. L. (2006) Rhodopsin self-associates in asolectin liposomes, *Proc Natl Acad Sci U S A.* **103**, 3060-5.

37. Kota, P., Reeves, P. J., Rajbhandary, U. L. & Khorana, H. G. (2006) Opsin is present as dimers in COS1 cells: Identification of amino acids at the dimeric interface, *Proc Natl Acad Sci U S A*.

38. Ernst, O. P., Gramse, V., Kolbe, M., Hofmann, K. P. & Heck, M. (2007) Monomeric G protein-coupled receptor rhodopsin in solution activates its G protein transducin at the diffusion limit, *Proc Natl Acad Sci U S A*. **104**, 10859-64.

39. Barth, A. & Zscherp, C. (2002) What vibrations tell us about proteins, *Q Rev Biophys.* **35**, 369-430.

40. Lavoie, H., Desbat, B., Vaknin, D. & Salesse, C. (2002) Structure of rhodopsin in monolayers at the air-water interface: a PM-IRRAS and X-ray reflectivity study, *Biochemistry.* **41**, 13424-34.

41. Rajan, R. S., Illing, M. E., Bence, N. F. & Kopito, R. R. (2001) Specificity in intracellular protein aggregation and inclusion body formation, *Proc Natl Acad Sci U S A.* **98**, 13060-5.

42. Kayed, R., Head, E., Thompson, J. L., McIntire, T. M., Milton, S. C., Cotman, C. W. & Glabe, C. G. (2003) Common structure of soluble amyloid oligomers implies common mechanism of pathogenesis, *Science.* **300**, 486-9.

43. LeVine, H., 3rd (1993) Thioflavine T interaction with synthetic Alzheimer's disease beta-amyloid peptides: detection of amyloid aggregation in solution, *Protein Sci.* **2**, 404-10.

44. Naiki, H., Higuchi, K., Hosokawa, M. & Takeda, T. (1989) Fluorometric determination of amyloid fibrils in vitro using the fluorescent dye, thioflavin T1, *Anal Biochem.* **177**, 244-9.

45. Tao, Y. X. & Conn, P. M. (2014) Chaperoning G protein-coupled receptors: from cell biology to therapeutics, *Endocr Rev.* **35**, 602-47.

Figure Legends

Fig. 1. (A-C) UV/vis absorbance spectroscopy conducted on purified untagged (A), CFP-tagged (B), or YFP-tagged (C) opsin reconstituted with 9-*cis* retinal. Absorbance spectra were obtained for unbleached samples using the buffer as the blank (solid line) and bleached samples using the unbleached sample as the blank (dotted line). (D-F) MII decay of untagged (D), CFP-tagged (E), or YFP-tagged (F) isorhodopsin determined by dequenching of tryptophan fluorescence. Curves were fit by non-linear regression assuming first-order reaction kinetics to determine the time constant (τ). The mean values for time constants are shown with the standard deviation and number of experiments (n).

Fig. 2. (A-H) Confocal microscopy of HEK293 cells expressing YFP-tagged opsins (green): WT (A, E), G188R (B, F), P23H (C, G), or WT opsin with an ER retention sequence (WT-KKYL) (D, H). Cells were stained either with the plasma membrane marker WGA (A-D) or with the ER marker DsRed2-ER (E-F), which is shown in red. DAPI staining is shown in blue. Scale bar, 10 μm. (I-L) FRET between coexpressed CFP- and YFP- tagged WT (I), G188R (J), P23H (K), WT-KKYL (L) opsin. Cell suspensions were excited at 425 nm. Emission spectra from untreated (blue), DM treated (red), and SDS treated (green) cells are shown. FRET is evident by the sensitized emission peak at 527 nm and dequenching of the CFP emission peak at 474 nm upon detergent treatment.

Fig. 3. (A) Epifluorescence and (B) FTIR image of HEK293 cells expressing G188R opsin tagged with YFP. The FTIR image represents the relative β-sheet content at each pixel as

calculated by the β-sheet/amide I ratio. High levels of β-sheet content (red) overlap with regions of high YFP fluorescence. Scale bar, 20 μm. (C-H) FTIR and second derivative spectra in the amide I region. (C, D) Spectra obtained from untransfected cells and cells expressing YFP-tagged WT opsin, untagged WT opsin, or YFP alone. (E, F) Spectra obtained from cells expressing YFP-tagged WT, G188R, P23H, or WT-KKYL opsin. (G, H) Spectra obtained from cells expressing untagged WT, G188R, or P23H opsin. Full spectra are shown in Supplemental Figs. S1-S3.

Figure 1

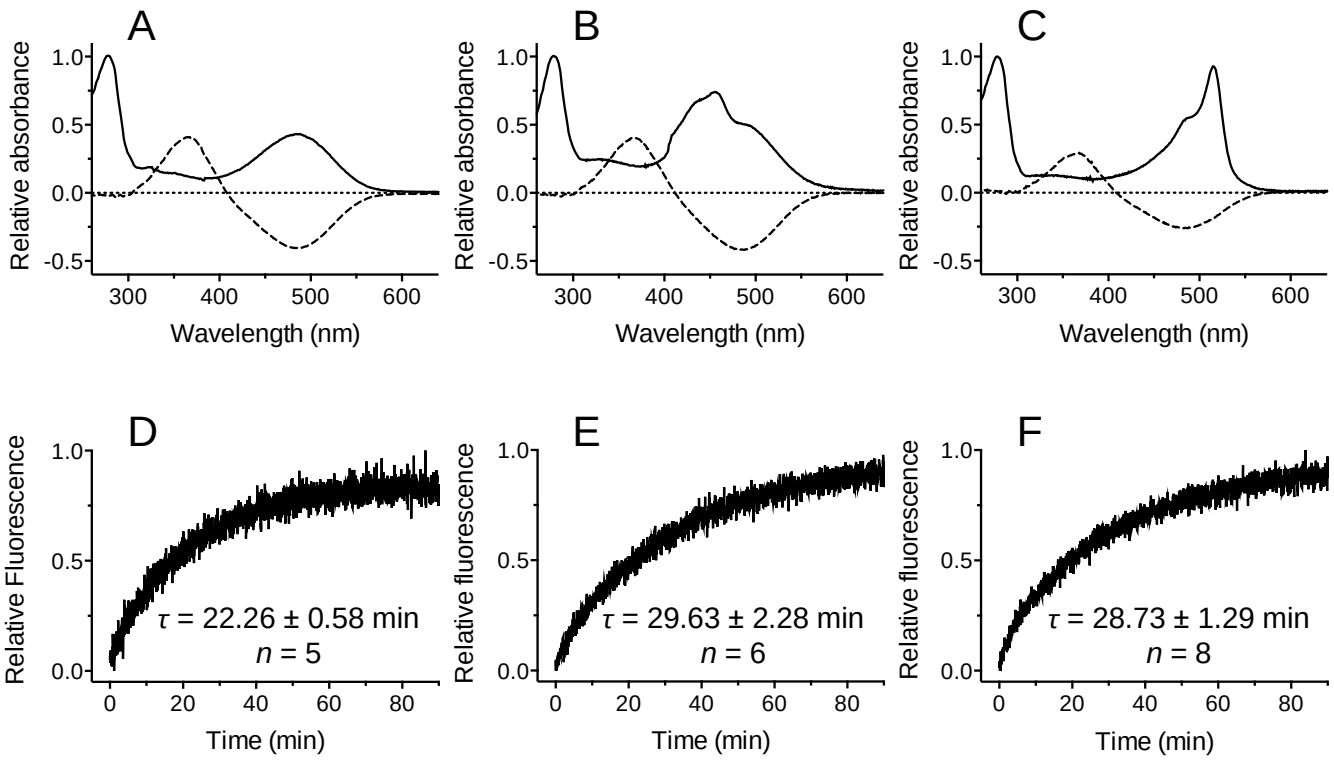
A
B
C
Relative absorbance
1.0
0.5
0.0
-0.5
300
400
500
600
Wavelength (nm)
D
E
F
Relative Fluorescence
Relative fluorescence
0.0
0.5
1.0
0
20
40
60
80
Time (min)
τ = 22.26 ± 0.58 min
n = 5
τ = 29.63 ± 2.28 min
n = 6
τ = 28.73 ± 1.29 min
n = 8

Figure 2

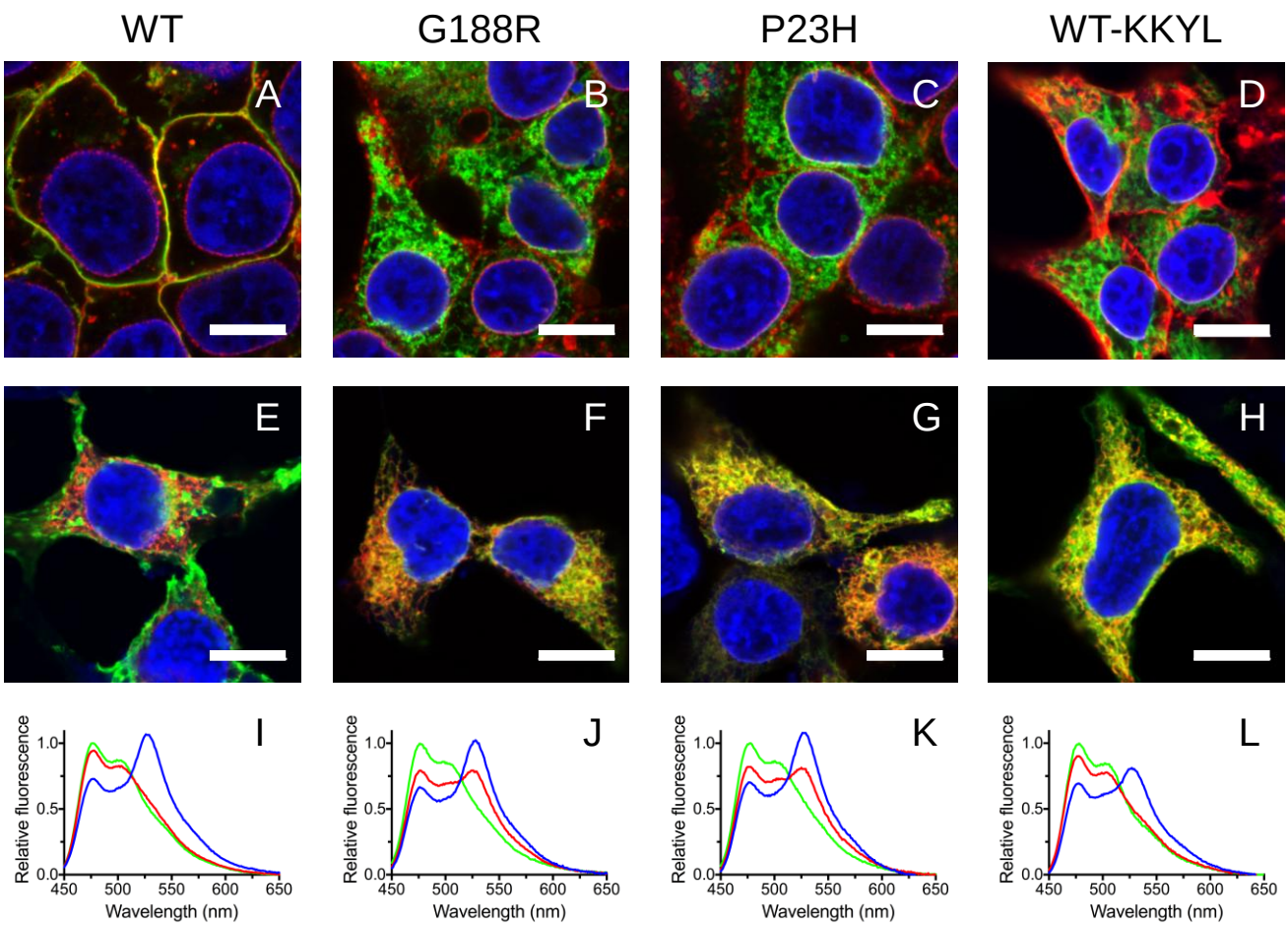
WT
G188R
P23H
WT-KKYL
A
B
C
D
E
F
G
H
I
J
K
L
Relative fluorescence
Wavelength (nm)
0.0
0.5
1.0
450
500
550
600
650

Figure 3

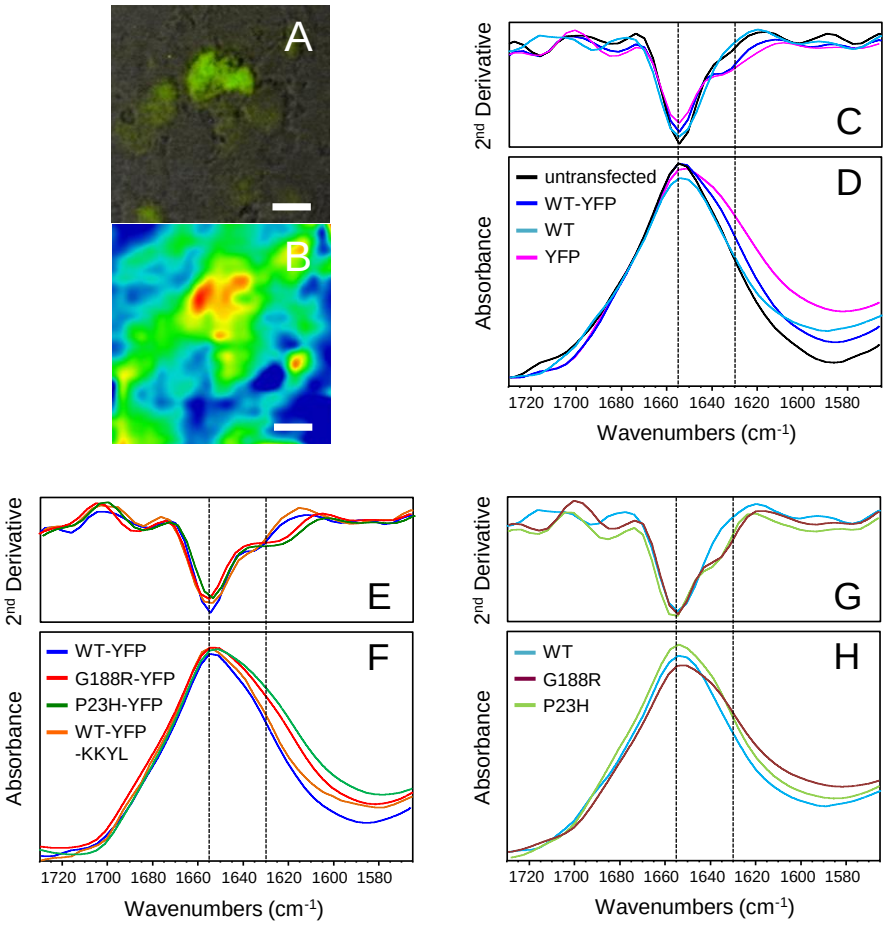
A
B
C
D
2nd Derivative
Absorbance
untransfected
WT-YFP
WT
YFP
1720 1700 1680 1660 1640 1620 1600 1580
Wavenumbers (cm-1)
E
F
WT-YFP
G188R-YFP
P23H-YFP
WT-YFP
-KKYL
G
H
WT
G188R
P23H

HIGHLIGHTS

- The effect of toxofilin on G-actin was studied with spectroscopy techniques.
- Toxofilin can effectively bind to non-parasitic actin monomers.
- G-actin and toxofilin interact with 2:1 stoichiometry.
- The nucleotide binding cleft is shifted to a closed structure due to toxofilin.
- The actin monomers are thermodynamically more stable in the presence of toxofilin.